Stanford Exploration Project, Report 129, May 6, 2007, pages 179–200

Anisotropic migration velocity analysis from residual moveout transformation in angle-domain common-image gathers

Pierre Jousselin and Biondo Biondi

ABSTRACT

We present the application of anisotropic migration velocity analysis (MVA) on synthetic data and on a real dataset acquired in the North Sea. The method we use to estimate anisotropic migration velocities is based on the computation and analysis of angle-domain common-image gathers (ADCIGs) in conjunction with anisotropic wavefield-continuation migration. Assuming flat reflectors and vertically transversely isotropic (VTI) media, we compute anisotropic velocity spectra from a residual moveout (RMO) transformation, based on the theoretical expression of the RMO in anisotropic ADCIGs as a function of perturbations in migration velocities.

In the first part of this paper, we briefly present the theory of ADCIGs and the derivation of the mathematical expression of the RMO function. In the second part, we analyze synthetic data with the method we propose to estimate anisotropic migration velocities. We demonstrate that our method is unable to resolve vertical velocities but nevertheless accurately estimates horizontal and normal moveout (NMO) velocities even for significant perturbations in the velocity model, provided the range of aperture angle is not too small. In the last part of this paper, we demonstrate on real data the validity of our estimation method, by showing it indicates the presence of velocity anellipticity in layers stratigraphically interpreted as anisotropic and for which well data do not match seismic data migrated under the assumption of isotropy.

INTRODUCTION

Since approximating the subsurface as an isotropic medium can be geologically unrealistic and since isotropic migration methods can give results inconsistent with well data, anisotropic migration has become an important focus of research and is now widely used. However, superior image quality and accurate reflector positioning require good estimates of anisotropic parameters.

Today, migration velocity analysis (MVA) is most commonly employed to estimate isotropic migration velocity in complex media. However, it is still less mature for anisotropic applications, and most recent work has developed anisotropic MVA only in conjunction with Kirchhoff migration (Tsvankin, 2001). The mathematical relationship that links residual moveout (RMO) in anisotropic angle-domain common-image gathers (ADCIGs) to anisotropic migration velocity errors (Biondi, 2005a,b) opens the way to new anisotropic MVA methods that

can be performed in conjunction with wavefield-continuation migration. These methods have the great advantage of being based on migrated gathers and allow the iterative estimation of anisotropic migration velocities.

In this paper, we present the results from computing anisotropic velocity spectra from RMO transformation in anisotropic ADCIGs assuming flat reflectors and vertically transversely isotropic (VTI) media. In the first part, we briefly present the theory of ADCIGs and the derivation of the mathematical expression of the RMO function. In the second part, we perform anisotropic MVA on synthetic data and analyze the accuracy and convergence of our estimation method. We demonstrate it does not resolve vertical velocities but nevertheless accurately estimates the horizontal and NMO velocities, even for significant perturbations, provided the range of aperture angle is not too small. We also show that when computing anisotropic velocity spectra as few approximations as possible must be made in order to attain accurate parameter estimates. In the last part, we perform anisotropic MVA on a real data set acquired in the North Sea. We demonstrate the validity of the method by showing it indicates the presence of velocity anellipticity in the layers stratigraphically interpreted as anisotropic, and for which well data do not match seismic data migrated under the assumption of isotropy.

RESIDUAL MOVEOUT IN ANISOTROPIC ADCIGS

In this section, we briefly present the theory of ADCIGs (Rickett and Sava, 2002; Sava and Fomel, 2003; Biondi and Tisserant, 2004) and the derivation of the mathematical expression of RMO in anisotropic ADCIGs as a function of errors in anisotropic velocity parameters (Biondi, 2005a,b; Jousselin and Biondi, 2006).

Generalized migration

Anisotropic ADCIGs are based on the generalization of integral migration to the computation of a prestack image that includes the subsurface-offset dimension (h_ξ) in addition to the usual image depth (z_ξ) and midpoint (m_ξ). Figure 1 illustrates the subsurface-offset dimension: the image point $\left(m_\xi, h_\xi, z_\xi\right)$ belongs to the migration response of an impulse recorded at midpoint m_D, surface offset h_D and travel time t_D, provided that the travel time along the source and receiver paths (of length L_s and L_r, respectively) is equal to t_D.

Computation of ADCIGs

In 2-D, ADCIGs are computed for each midpoint by applying a slant-stack decomposition to the prestack image along the subsurface-offset axis. The kinematics of the angle-domain transformation are defined by the following change of variable:

$$\widehat{\gamma} = \arctan \left. \frac{\partial z_\xi}{\partial h_\xi} \right|_{m_\xi = \overline{m}_\xi}, \tag{1}$$

$$z_{\widehat{\gamma}} = z_\xi - h_\xi \tan \widehat{\gamma}, \tag{2}$$

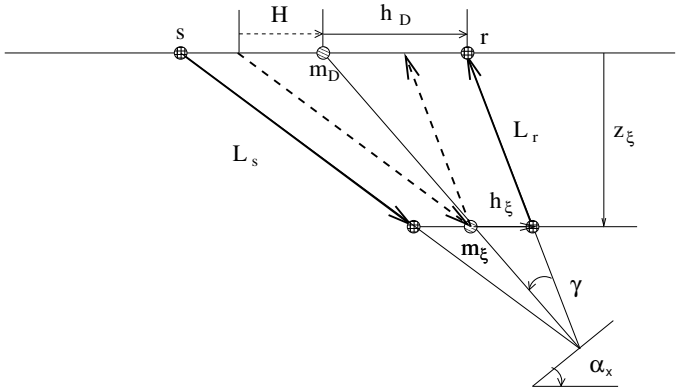

Figure 1: Illustration of generalized migration, where the prestack image is a function of the subsurface offset and γ and α_x are the group aperture and dip angles, respectively. pierre1-imp-resp [NR]

where $z_{\widehat{\gamma}}$ is the transformed image-point depth. Assuming flat reflectors and VTI media, Biondi (2005a) demonstrates that the angle $\widehat{\gamma}$ is equal to the phase aperture angle $\widetilde{\gamma}$, thereby simplifying equations 1 and 2:

$$\widetilde{\gamma} = \arctan \left. \frac{\partial z_\xi}{\partial h_\xi} \right|_{m_\xi = \overline{m}_\xi}, \tag{3}$$

$$z_{\widetilde{\gamma}} = z_\xi - h_\xi \tan \widetilde{\gamma}. \tag{4}$$

RMO analysis in ADCIGs

When the migration velocity is correct and the image is focused at zero subsurface offset, transformation to the angle domain does not change the image-point depth and the reflections are imaged at the same depth for all aperture angles ($z_{\widetilde{\gamma}} = z_\xi = const$). As a consequence, when migrated with the correct migration velocity, reflectors are mapped flat in ADCIGs. In contrast, when the reflections are not focused at zero offset, transformation to the angle domain maps the events to different depths for each different angle. The image-depth variability with aperture angle is described by the RMO function, which we want to measure and quantify as a function of the perturbation in anisotropic parameters. Below, we summarize the approach given by Biondi (2005a) to derive the expression of RMO in anisotropic ADCIGs. It consists of approximating the RMO by the first-order Taylor series expansion about the correct migration velocity.

The notation used in Biondi (2005a) is the following: the VTI velocity function parameterization is $\mathbf{V} = (V_V, V_H, V_N)$, where V_V is the velocity of a vertical ray, V_H is the velocity of a horizontal ray and V_N is the NMO velocity. It is equivalent to Thomsen's parameterization $\mathbf{V} = (V_V, \epsilon, \delta)$, since $V_H = V_V\sqrt{1+2\epsilon}$ and $V_N = V_V\sqrt{1+2\delta}$.

We define the perturbations in the VTI velocity function as a three-component vector $\boldsymbol{\rho}$= $\left(\rho_{V_V}, \rho_{V_H}, \rho_{V_N}\right)$, where each component is a multiplicative factor for each migration velocity. The vector generates a perturbed velocity field, ${}_\rho\mathbf{V}$ defined by ${}_\rho\mathbf{V} = \left({}_\rho V_V, {}_\rho V_H, {}_\rho V_N\right) = \left(\rho_{V_V} V_V, \rho_{V_H} V_H, \rho_{V_N} V_N\right)$.

From the analytic expression of the impulse response (derived from Figure 1) and geometric interpretation of the angle-domain transformation, Biondi (2005a) derives the first-order

derivatives of the image depth in the angle domain with respect to anisotropic parameter perturbations:

$$\frac{\partial z_{\widetilde{\gamma}}}{\partial \rho_i} = -z_\xi \frac{(1+\tan\widetilde{\gamma}\tan\gamma)}{S(\gamma)} \frac{\partial S}{\partial \rho_i}, \tag{5}$$

where S is the slowness along the source and receiver rays.

Similarly, because residual moveout Δz_{RMO} is defined as the difference between the reflector movement at finite angle ($\widetilde{\gamma}$) and the reflector movement at normal incidence ($\widetilde{\gamma}=0$), from equation 5, we can express the first-order derivatives of the residual moveout with respect to anisotropic parameter perturbations:

$$\frac{\partial \Delta z_{\text{RMO}}}{\partial \rho_i} = \left.\frac{\partial z_{\widetilde{\gamma}}}{\partial \rho_i}\right|_{\widetilde{\gamma}} - \left.\frac{\partial z_{\widetilde{\gamma}}}{\partial \rho_i}\right|_{\widetilde{\gamma}=0}. \tag{6}$$

The residual moveout Δz_{RMO} is eventually approximated by the first-order Taylor series expansion about the correct migration velocity ($\rho = \mathbf{1}$). The linearized expression is the following:

$$\Delta z_{\text{RMO}} = \left.\frac{\partial \Delta z_{\text{RMO}}}{\partial \rho_{V_V}}\right|_{\widetilde{\gamma},\rho=\mathbf{1}} \left(\rho_{V_V}-1\right) + \left.\frac{\partial \Delta z_{\text{RMO}}}{\partial \rho_{V_H}}\right|_{\widetilde{\gamma},\rho=\mathbf{1}} \left(\rho_{V_H}-1\right) + \left.\frac{\partial \Delta z_{\text{RMO}}}{\partial \rho_{V_N}}\right|_{\widetilde{\gamma},\rho=\mathbf{1}} \left(\rho_{V_N}-1\right). \tag{7}$$

Synthetic examples

The accuracy of the RMO function predicted from equations 5 to 7 is demonstrated in Biondi (2005a,b), for a large range of velocity perturbations. Figure 2 presents the ADCIGs obtained when a flat reflector is migrated with inaccurate migration velocity models. The data were modeled using the anisotropic parameters of the Taylor Sand (Tsvankin, 2001): $\epsilon = 0.110$ and $\delta = -0.035$. It was then migrated using: a) a velocity uniformly perturbed by $\rho_V = 0.99$, b) a velocity uniformly perturbed by $\rho_V = 0.9$, and c) an isotropic velocity with the correct vertical velocity. The predicted residual moveouts derived from equations 5 to 7 are superimposed. The solid line was computed when $\tan\gamma$ was derived from $\tan\widetilde{\gamma}$ by applying equation A-2, whereas the dashed line was computed using the approximation $\tan\gamma \approx \tan\widetilde{\gamma}$.

The predicted RMO functions accurately track the actual RMO functions when the perturbations are sufficiently small to be within the linearization accuracy range (Figure 2-a). Even when the perturbations are large (Figures 2-b and 2-c) and cause a substantial RMO, the predicted RMO functions are excellent approximations of the true RMO functions. In contrast, the approximation of the group angles with the phase angles (dashed lines in the figures) seriously lowers the accuracy of the predicted RMO functions.

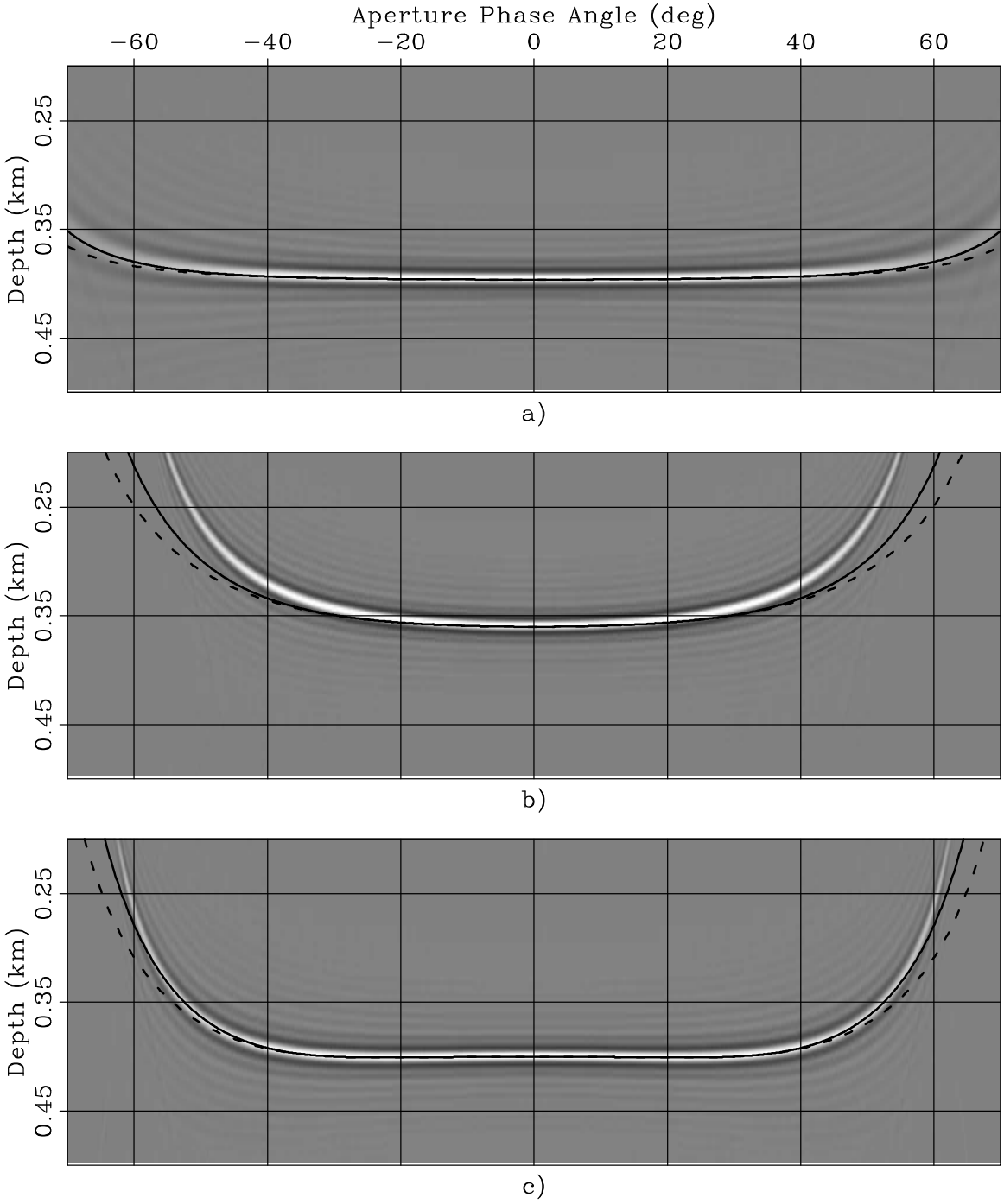

Figure 2: ADCIG obtained when data modeled using constant anisotropic parameters (Taylor Sand) have been migrated using: a) a velocity uniformly perturbed by $\rho_V = 0.99$, b) a velocity uniformly perturbed by $\rho_V = 0.9$, and c) an isotropic velocity with the correct vertical velocity. Superimposed onto the images are the RMO functions computed using equations 5 to 7. The solid line was computed when $\tan\gamma$ was derived from $\tan\widetilde{\gamma}$ by applying equation A-2, whereas the dashed line was computed with the approximation $\tan\gamma \approx \tan\widetilde{\gamma}$. pierre1-Aniso-rmo [ER]

ANISOTROPIC MIGRATION VELOCITY ANALYSIS OF SYNTHETIC DATA FROM RMO TRANSFORMATION IN ANISOTROPIC ADCIGS

In the preceding section, we derived the expression of the RMO in anisotropic ADCIGs as a function of anisotropic parameter perturbations and demonstrated its accuracy for different types of velocity model perturbations. In this section, we perform anisotropic MVA on the same synthetic data and analyze the accuracy and convergence of our estimation method. We also illustrate caveats in the computation of anisotropic velocity spectra and demonstrate that as few approximations as possible should be made in order to attain accurate anisotropic parameter estimates.

Estimation of the vertical velocity

First, we show that for flat reflectors and VTI media, vertical velocities cannot be estimated from reflection seismic data only. These results are consistent with Tsvankin (2001), who shows that P-wave signatures depend only on two combinations of V_V, δ and ϵ, and that vertical velocities cannot be estimated from reflection seismic data only.

For elliptical media, we demonstrate that the first-order derivative of the image-point depth with respect to vertical velocity perturbations is independent of the aperture angle so that the residual moveout is independent of the vertical velocity perturbations:

$$\frac{\partial z_{\tilde{\gamma}}}{\partial \rho_{V_V}} = -z_\xi, \tag{8}$$

$$\frac{\partial \Delta z_{\text{RMO}}}{\partial \rho_{V_V}} = \frac{\partial z_{\tilde{\gamma}}}{\partial \rho_{V_V}}\bigg|_{\tilde{\gamma}} - \frac{\partial z_{\tilde{\gamma}}}{\partial \rho_{V_V}}\bigg|_{\tilde{\gamma}=0} = 0. \tag{9}$$

As a consequence, vertical velocity perturbations cannot be estimated from RMO transformation.

For anelliptical media, we show numerically that the first-order derivative of the RMO with respect to vertical velocity perturbations is not significantly different from zero and does not allow the estimation of vertical velocity perturbations.

Estimation of the horizontal and NMO velocities

Since the vertical velocities cannot be estimated from RMO transformations in anisotropic ADCIGs, we computed the semblance values for ρ_{V_H} and ρ_{V_N} only. Figure 3 illustrates the velocity spectra computed at the image depth for the various ADCIGs illustrated in Figure 2. The various semblance panels are computed for various aperture angle ranges (30°, 45° and 60°). When computing the semblance of a velocity model, the first-order derivatives in equation 5 are computed around that velocity model, not around the one that was used for the migration. The group aperture angles are computed from phase aperture angles using equation A-2. The

parameterization of the estimated anisotropic parameters is done with the perturbations in the horizontal (ρ_{V_H}) and NMO velocities (ρ_{V_N}). For visualization purposes, Figure 4 illustrates the same semblance panels, but this time, the axes ρ_{V_H} and ρ_{V_N} have been normalized by the correct perturbations in the anisotropic migration velocities. As a consequence, in Figure 4, the true velocities lie in the center of the semblance panels. Several conclusions can be drawn from Figure 4.

- **Effect of the aperture angle**: As the range of the aperture angle increases, so does the residual moveout and the information about the true velocity model. As a consequence, the estimates of the anisotropic parameters become more accurate. Furthermore, as the range of the aperture angle increases, the relative constraints on the horizontal and NMO velocities become more even.

- **Accuracy of the estimation method**: For aperture angles around 30°, Figure 4 illustrates that the velocity perturbations are unresolved (especially ρ_{V_H}). For aperture angles larger than 45°, the largest semblance values are found close to the center of the semblance panels, demonstrating the accuracy of the estimation method. However, the largest semblance values are not exactly centered, but slightly shifted toward the upper left, indicating that the anisotropic migration velocities tend to be underestimated. This is consistent with Figure 2 that illustrates that the predicted RMO functions underestimate the absolute value of the true RMOs.

- **Convergence of the estimation method**: Table 1 displays the values of $\rho_{V_H} - 1$ and $\rho_{V_N} - 1$ for the maximum semblance velocity models, as a function of the aperture angle range. These quantities are equivalent to the percentage error in V_H and V_N estimates. Table 1 indicates that starting from an isotropic model or a uniform perturbation of $\rho_V = 0.9$, the estimation method improves the estimates of V_H and V_N by reducing the percentage errors to less than 2%. However, it also shows that for a velocity model uniformly perturbed by $\rho_V = 0.99$, the estimation method may neither converge nor improve the accuracy of the migration velocity model since for a 60° aperture angle range, the estimation error is still of the order of 1% (i.e. the starting velocity model error).

- **Trade-off between the anisotropic migration velocities**: Figure 4 shows a negative trade-off between ρ_{V_H} and ρ_{V_N}, because a perturbation in V_H can be balanced by a perturbation of the opposite sign in V_N, and result in a very small net change in the predicted RMO function. This negative trade-off has an important practical consequence: it justifies the joint-estimation of ρ_{V_H} and ρ_{V_N}. The successive estimation of ρ_{V_H} and ρ_{V_N} may lead to a much poorer convergence rate.

Caveats in the computation of velocity spectra

Eventually, we illustrate the caveats in the computation of anisotropic velocity spectra and demonstrate that as few approximations as possible should be made in order to attain accurate anisotropic parameter estimates. As equation 5 shows, the predicted RMO is a function

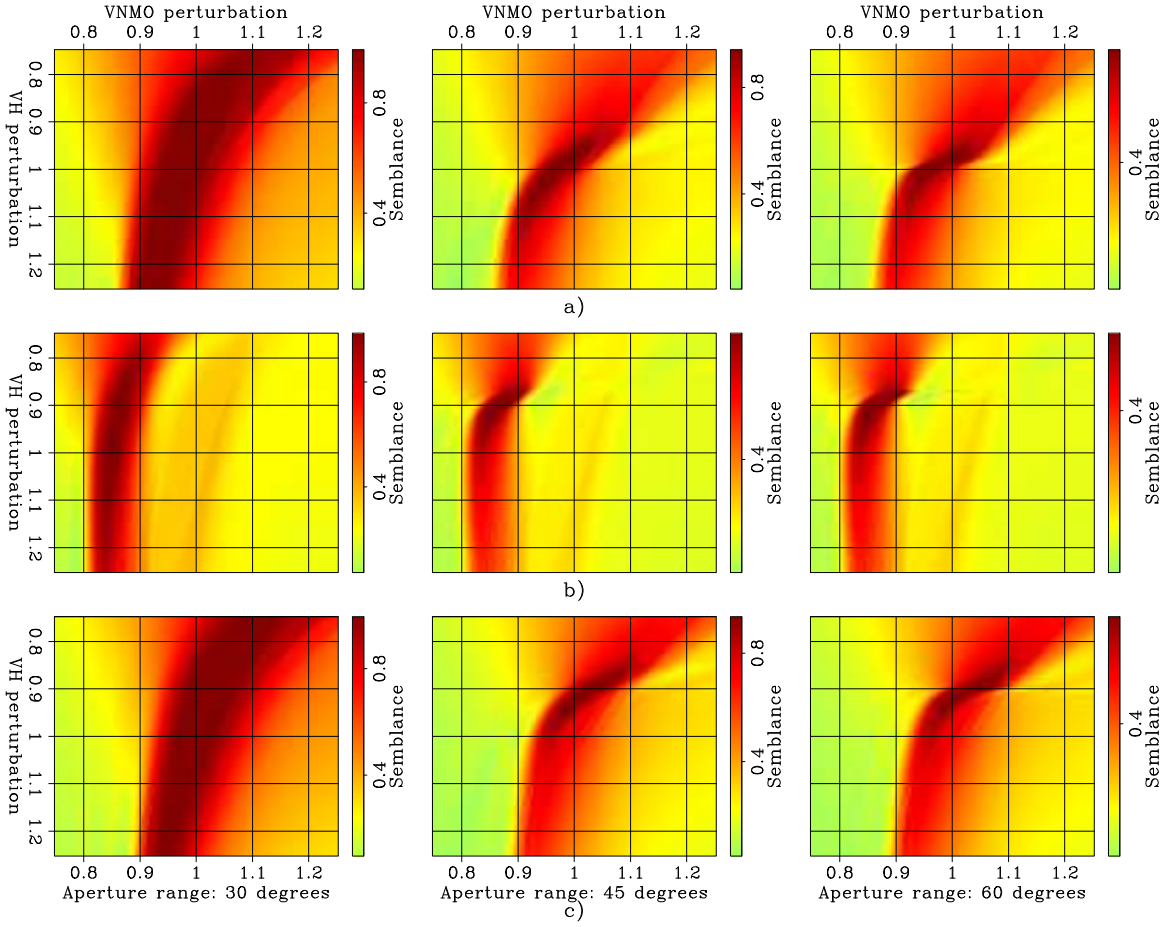

Figure 3: Velocity spectra obtained at the image depth when data modeled with a constant anisotropic velocity model (Taylor Sand) have been migrated using: a) a velocity uniformly perturbed by $\rho_V = 0.99$, b) a velocity uniformly perturbed by $\rho_V = 0.9$, and c) an isotropic velocity with the correct vertical velocity. The various semblance panels are computed for various aperture angle ranges (30°, 45° and 60° from left to right). The parameterization of the estimated anisotropic velocity model is done with the perturbations in the horizontal (ρ_{V_H}) and in the NMO velocity (ρ_{V_N}). The correct perturbation values are: a) $\rho_{V_H} = 0.99$ and $\rho_{V_N} = 0.99$, b) $\rho_{V_H} = 0.9$ and $\rho_{V_N} = 0.9$, and c) $\rho_{V_H} = 0.905$ and $\rho_{V_N} = 1.037$. pierre1-Comb-VelSpec-group [ER]

Velocity model perturbation	Initial perturbation	Range of aperture angles		
		[0,30]	[0,45]	[0,60]
1 % uniform perturbation	$(-1.0\%, -1.0\%)$	$(-3.5\%, +5.0\%)$	$(-2.5\%, +2.0\%)$	$(-1.0\%, +0.5\%)$
10 % uniform perturbation	$(-10.0\%, -10.0\%)$	$(-4.5\%, +7.0\%)$	$(-3.0\%, +0.0\%)$	$(-1.5\%, -1.5\%)$
Isotropic model with right V_V	$(-9.5\%, +3.7\%)$	$(+1.5\%, -3.5\%)$	$(-2.0\%, +1.5\%)$	$(+0.5\%, +0.0\%)$

Table 1: Values of $\left(\rho_{V_H} - 1, \rho_{V_N} - 1\right)$ for the maximum semblance velocity model, as a function of the aperture angle range.

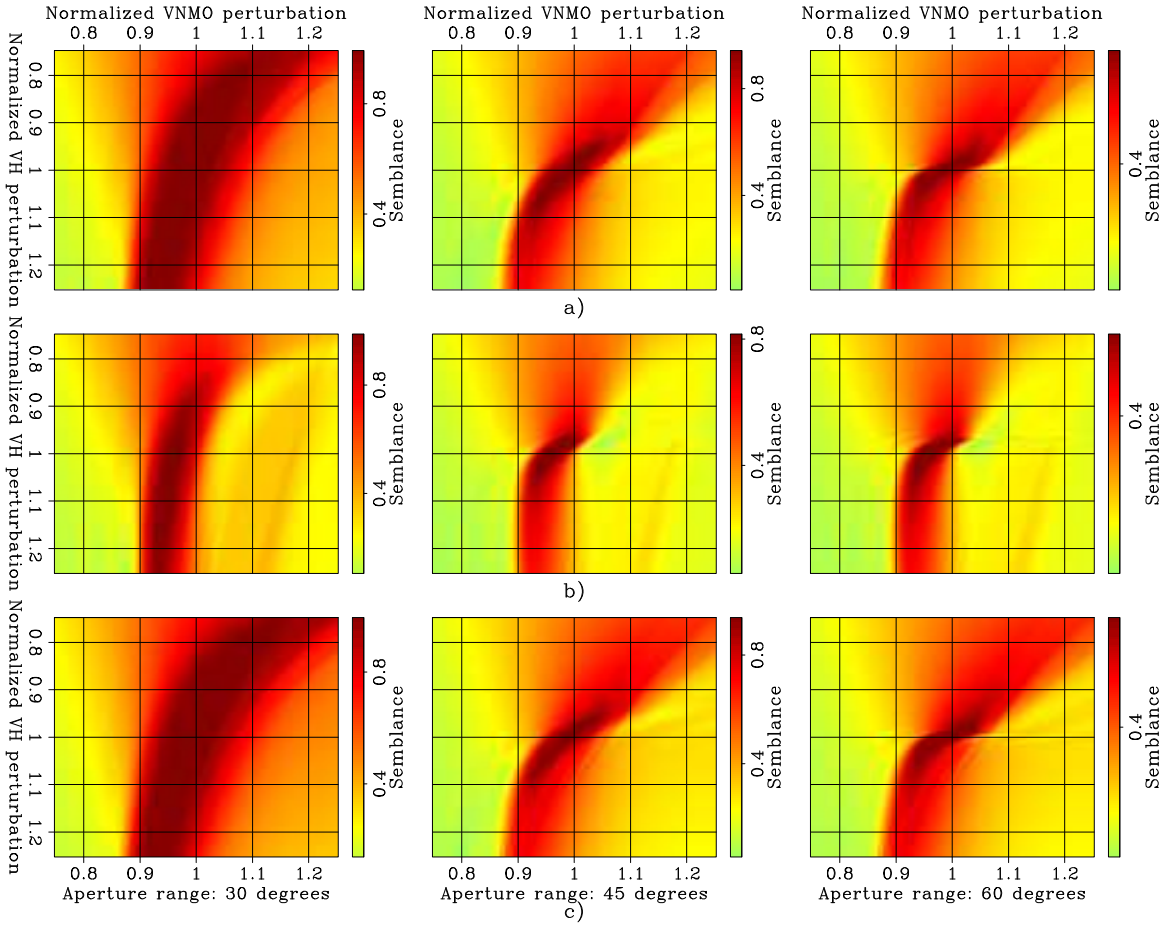

Figure 4: Velocity spectra obtained at the image depth when data modeled with a constant anisotropic velocity model (Taylor Sand) have been migrated using: a) a velocity uniformly perturbed by $\rho_V = 0.99$, b) a velocity uniformly perturbed by $\rho_V = 0.9$, and c) an isotropic velocity with the correct vertical velocity. The various semblance panels are computed for various ranges of aperture angles (30°, 45° and 60° from left to right). The parameterization of the estimated anisotropic velocity model is done with ρ_{V_H} and ρ_{V_N} by the correct perturbation values. pierre1-Comb-VelSpec-group_centrd [ER]

of both phase and group aperture angles. Phase aperture angles are computed by applying post-processing slant-stacks on the prestack migrated image (equation 3). Group aperture angles have to be derived from phase aperture angles. Figure 5 illustrates the velocity spectra computed when approximating the group aperture angles with the phase aperture angles. It shows the inaccuracy of the estimates of the anisotropic parameters for large velocity perturbations. Figure 6 illustrates the velocity spectra computed when the first-order derivatives in equation 5 are computed around the migration velocity model and not the velocity model whose semblance we compute. The group aperture angles are computed from phase aperture angles using equation A-2. Figure 6 illustrates the inaccuracy of the anisotropic parameter estimates for large velocity perturbations. It indicates that when computing velocity model semblances, first-order derivatives of the RMO functions have to be estimated independently for each velocity model.

ANISOTROPIC MIGRATION VELOCITY ANALYSIS ON REAL DATA FROM RMO TRANSFORMATION IN ANISOTROPIC ADCIGS

In this section, we perform anisotropic migration velocity analysis on real data and demonstrate the validity of our estimation method, by showing it indicates the presence of anellipticity in layers stratigraphically interpreted as anisotropic and for which well data do not match seismic data migrated under the assumption of isotropy. We first present the geologic setting and imaging challenges of the Alwyn field, where the data set was acquired. We then compute anisotropic velocity spectra.

Geologic setting

The Alwyn field is located in the UK sector of the North Sea, about 440 kilometers northeast from Aberdeen. The geologic setting is a tilted block structure with three reservoir formations (Figure 7): the Brent reservoir (top) produces oil, the Statfjord reservoir (middle) produces gas and the Triassic reservoir (bottom) produces oil. Existing 3D isotropic prestack time-migration (PSTM) and prestack depth-migration (PSDM) images are considered insufficient for structural understanding of the different fault blocks of this fluvial formation.

Imaging challenges

Several imaging challenges associated with Alwyn are well illustrated in Figure 8 that shows the seismic crossline of the migrated cube obtained by CGG in 2003 after isotropic Kirchoff prestack migration. It shows the following different challenges encountered in the area of interest:

- First, the reflectors and faults below the BCU horizon (strong reflector at around 3.5 km depth) are moderately well focused.

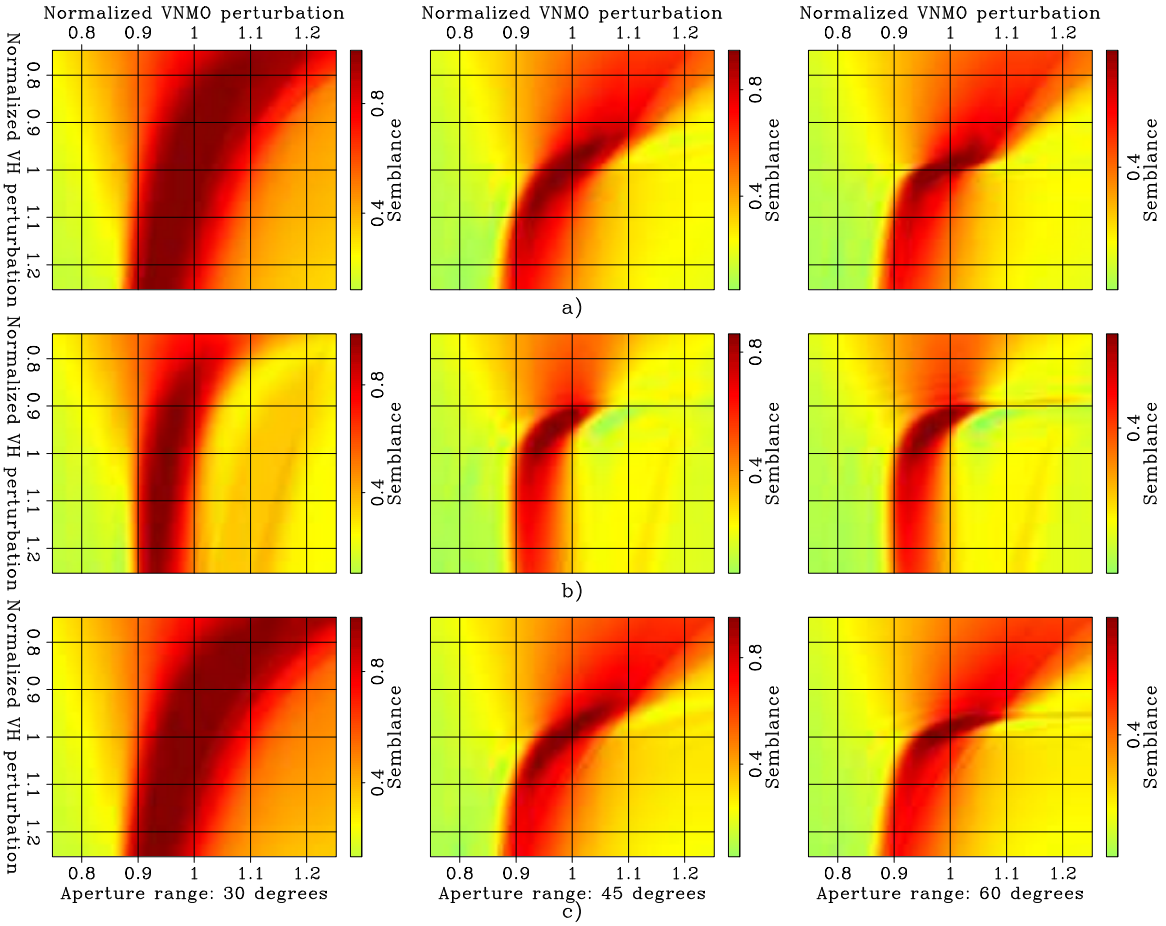

Figure 5: Velocity spectra obtained when the group aperture angles are approximated as equal to the phase aperture angles. The data have been modeled with a constant anisotropic velocity model (Taylor Sand) and then migrated using: a) a velocity uniformly perturbed by $\rho_V = 0.99$, b) a velocity uniformly perturbed by $\rho_V = 0.9$, and c) an isotropic velocity with the correct vertical velocity. The different semblance panels are computed for different ranges of aperture angles (30°, 45° and 60°, from left to right). The parameterization of the estimated anisotropic velocity model is done with ρ_{V_H} and ρ_{V_N} normalized by the correct perturbation values. pierre1-Comb-VelSpec-phase_centrd [ER]

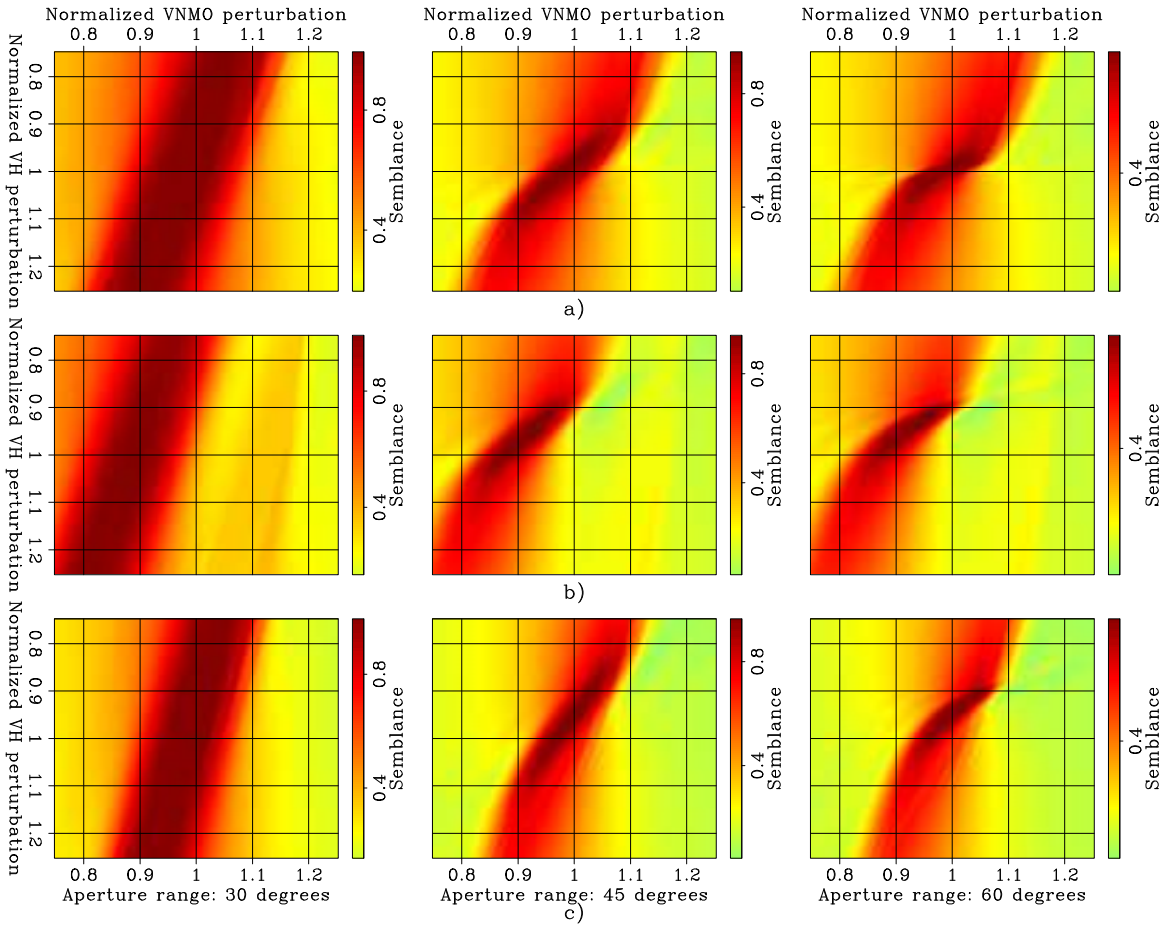

Figure 6: Velocity spectra obtained when the first-order derivatives in equation 5 are computed around the migration velocity model. The group aperture angles are computed from phase aperture angles using equation A-2. The data have been modeled with a constant anisotropic velocity model (Taylor Sand) and then migrated using: a) a velocity uniformly perturbed by $\rho_V = 0.99$, b) a velocity uniformly perturbed by $\rho_V = 0.9$, and c) an isotropic velocity with the correct vertical velocity. The different semblance panels are computed for different ranges of aperture angles (30°, 45° and 60°, from left to right). The parameterization of the estimated anisotropic velocity model is done with ρ_{V_H} and ρ_{V_N}, normalized by the correct perturbation values. pierre1-Comb-VelSpec-group_approx_centrd [ER]

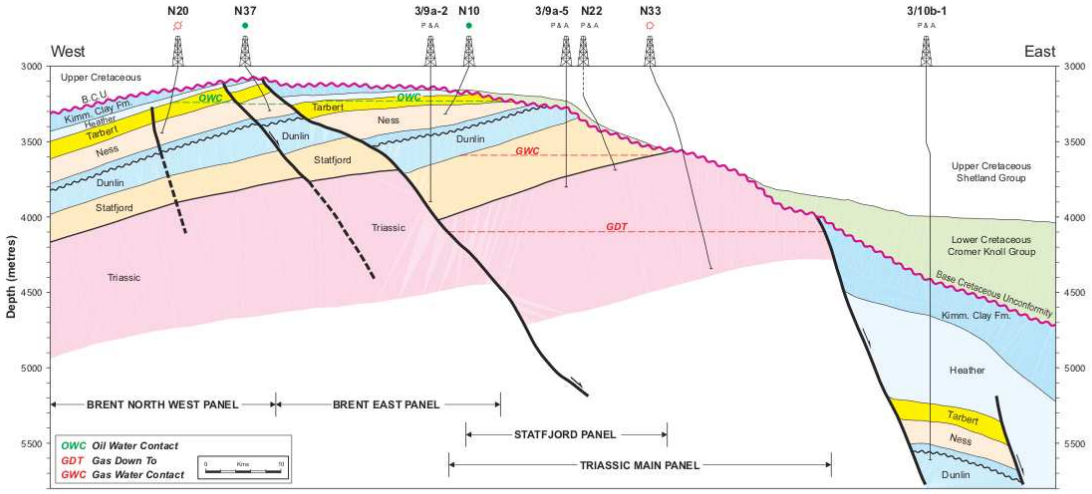

Figure 7: Geological section of the Alwyn field operated by TOTAL UK. pierre1-Section [NR]

- Second, a complex channel at around 1.0 km depth distorts the underlying horizons and especially the Balder horizon (strong and continuous reflector at around 1.5 km depth), affected by pull-ups (for example, at inlines 630, 660 and 700).
- Third, strong multiples contaminate the lower part of the image as well as strong migration smiles due to limited crossline acquisition aperture.

Furthermore, anisotropy is commonly observed in the North Sea. In the Alwyn field, the thick layer between the Top Chalk horizon (at around 2.2 km depth) and the BCU horizon is made of chalk, a sedimentary carbonate rock whose main mineral (calcite) has an anisotropic crystalline structure. The anisotropy of this layer, if not taken into account in the migration, can result in poor imaging of the underlying layers.

Description of the available data

TOTAL UK provided us with the data from the 2001 acquisition (preprocessed recently by Veritas), the isotropic interval velocity model developed by CGG in 2003, and the data from 15 nearby wells.

- **Acquisition area** In 2001, approximately 260 km^2 of 3D seismic full-fold data was acquired with an interleaved acquisition. The available seismic data spans 180 km^2.
- **2001 survey acquisition parameters** The main parameters of the acquisition are illustrated in Figure 9. The shotpoint interval is 18.75 meters. The bin size of the data preprocessed by Veritas in 2006 is 6.25 meters by 18.75 meters, corresponding to a stacking fold of 108.

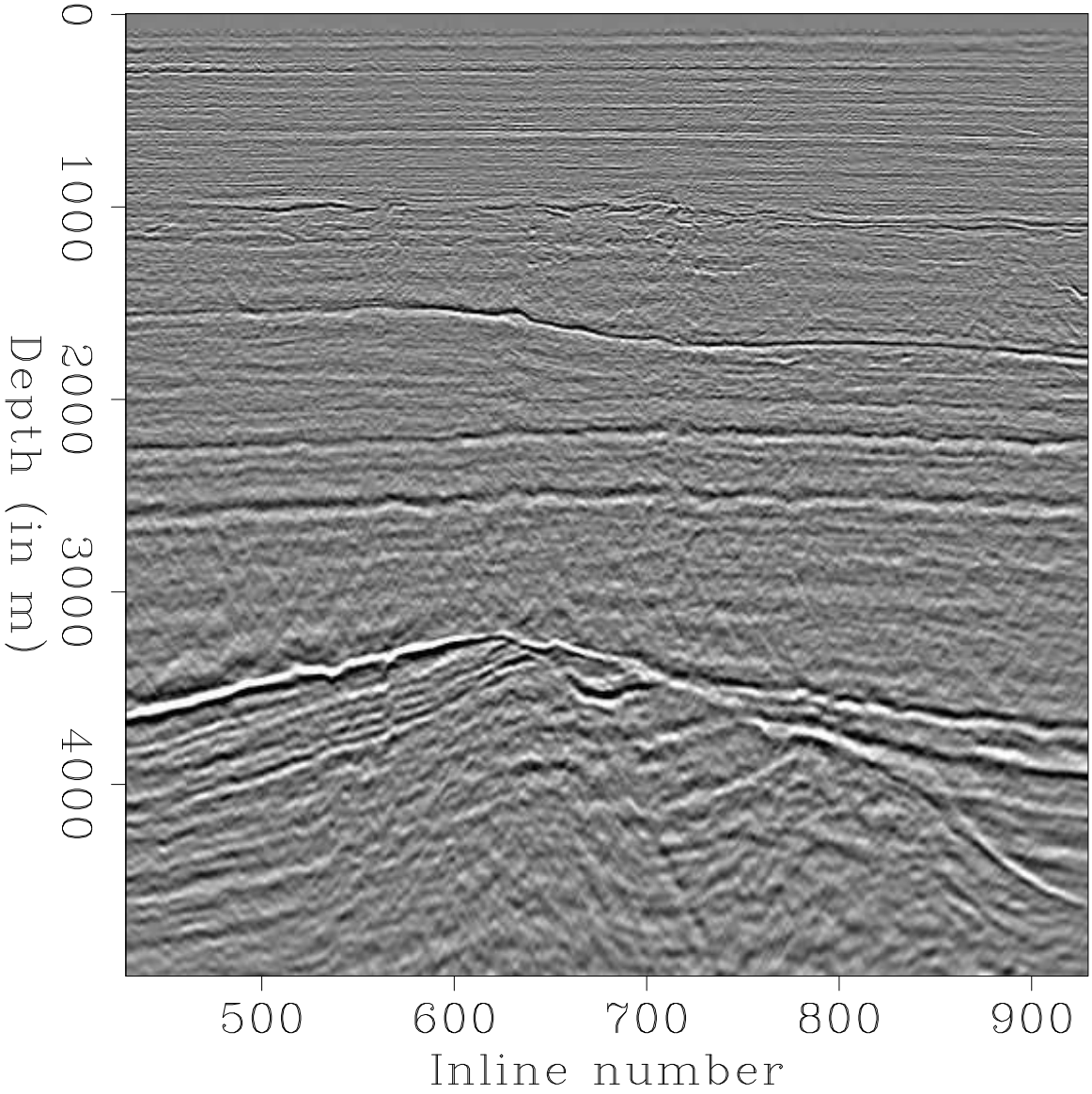

Figure 8: Crossline 1999 of CGG 2003 PSDM cube obtained after isotropic Kirchhoff prestack migration. The distance between two inlines is equal to 18.75m. pierre1-Section_Crossline_1999 [CR]

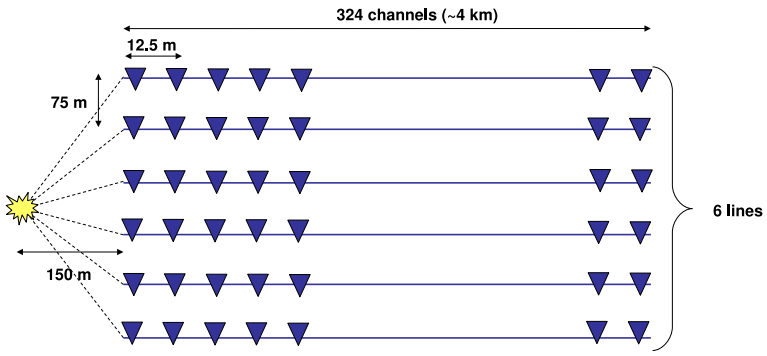

Figure 9: 2001 survey acquisition geometry. pierre1-Acquisition_parameters [NR]

- **Isotropic Velocity model** We were provided with the final isotropic interval velocity depth model computed by CGG. The blocky velocity model was first built in time using the interpreted time-horizons, the surface seismic stacking velocities and the compaction gradients given by the wells. It was then updated by layer-stripping. Two different updating methods were used. The first one was to compute CRP scans and perform normal-ray update. The second method was to pick residual curvature and perform multi-offset velocity updates. Figure 11 illustrates the final isotropic velocity model for Line 750.

Migration of the data

We restricted ourselves to 2D anisotropic migration velocity estimation and to mild dips. For that reason, we selected a line where crossline and inline dips are limited (Line 750 illustrated in Figure 10). As illustrated, the geologic structure along line 750 is relatively flat, and the assumption of flat reflectors is reasonable. This allows us to use the analytical expression of the RMO in ADCIGs presented by Biondi (2005b) and to compute anisotropic velocity spectra. Furthermore, it has the advantage of having a nearby well. This gives us useful vertical velocity constraints when building the anisotropic velocity model.

In our estimation procedure, we use an anisotropic source-receiver migration program and first perform an isotropic migration of the data starting from the interval vertical velocity model developed by CGG (Figure 11). The migration result is illustrated in the Figure 10.

Analysis of ADCIGs and computation of anisotropic velocity spectra

We compute ADCIGs from the prestack migrated image by applying post-processing slant stacks (Rickett and Sava, 2002; Sava and Fomel, 2003). The ADCIGs at three different locations are illustrated in Figure 12. It can be observed that up to 2 km depth, reflectors are imaged flat in ADCIGs, meaning that the migration velocity obtained by CGG is correct and that no anisotropy in those layers is needed. However, we can observe that below the Balder horizon (strong reflector at around 1.7 km depth), the reflectors start curving downward, indicating that the estimated isotropic migration velocity is larger than the true migration velocity. That

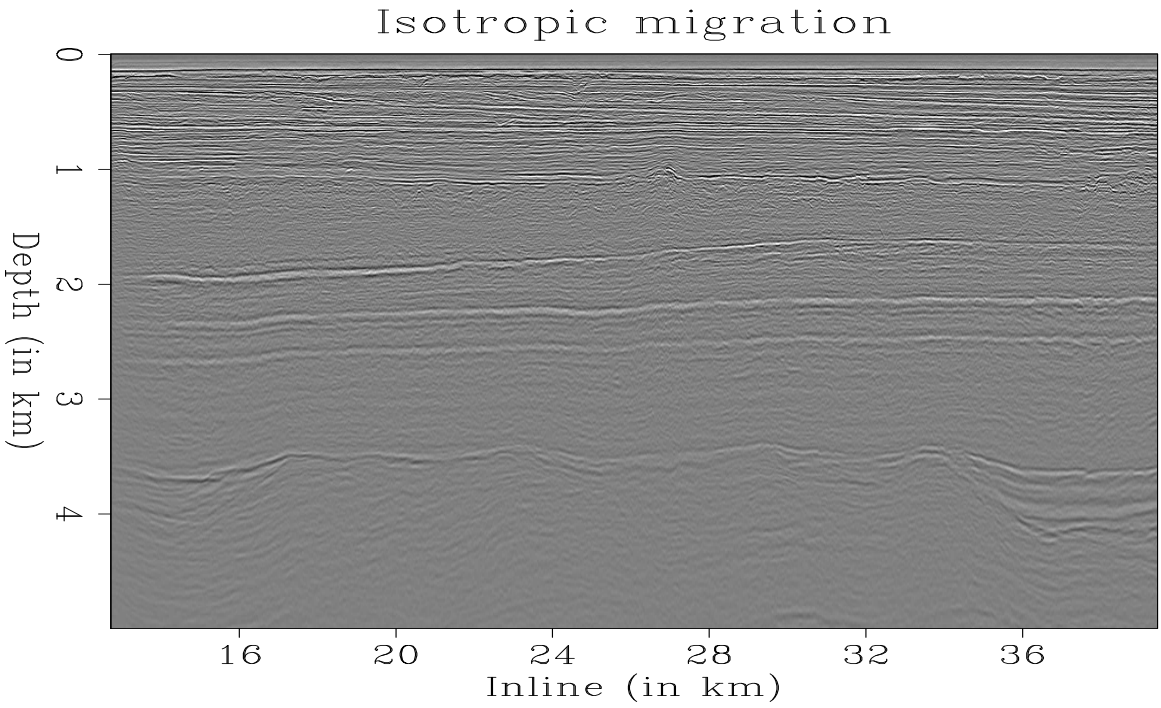

Figure 10: Line 750: Migration result obtained after isotropic source-receiver migration. pierre1-Section-iso-750 [CR]

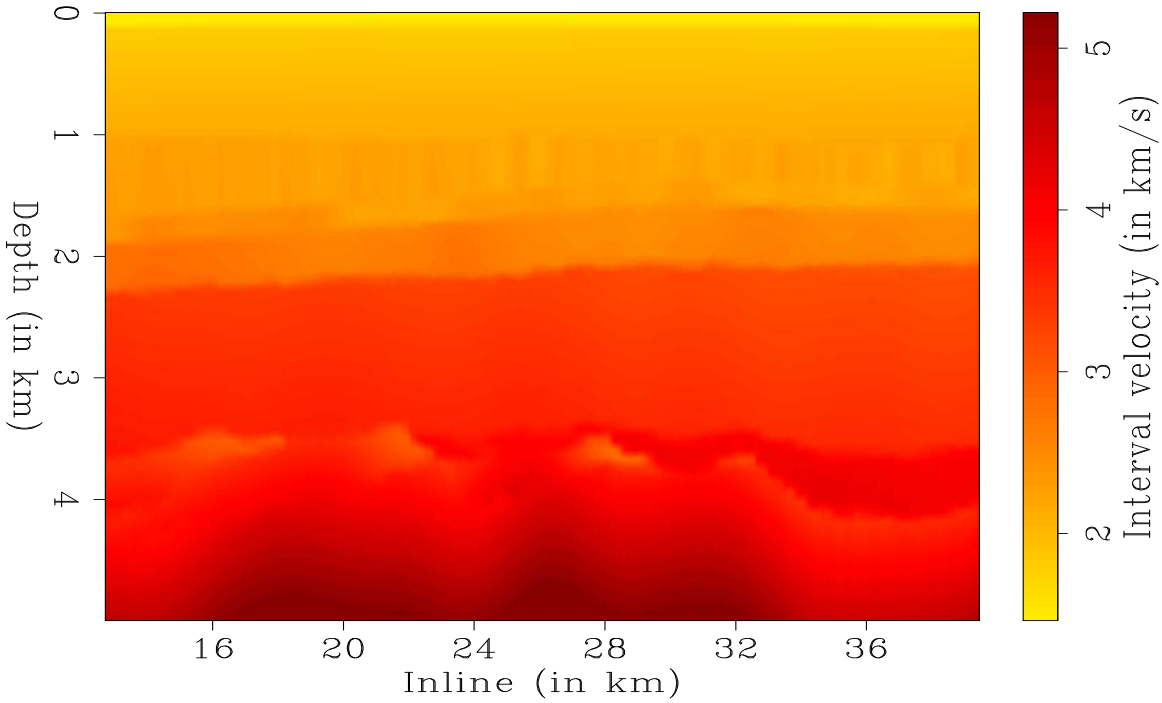

Figure 11: Line 750: Starting isotropic interval velocity model obtained by CGG (2003). pierre1-Velocity-750 [CR]

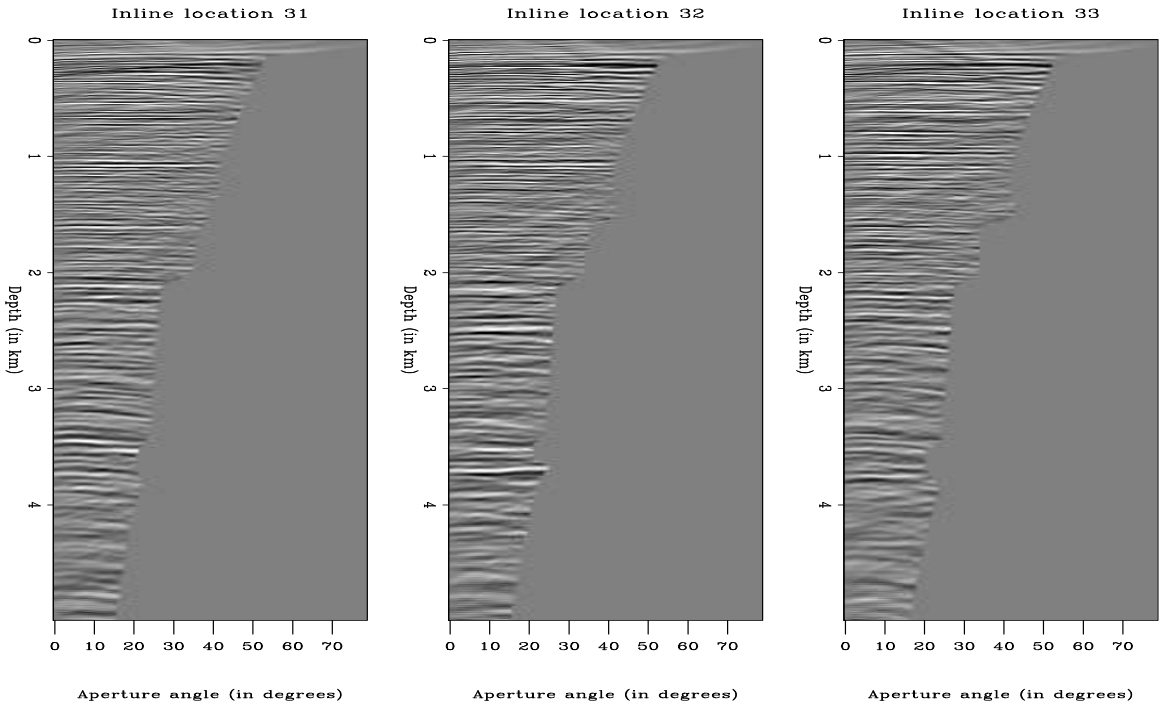

Figure 12: Line 750: ADCIGs at different locations obtained after isotropic migration. pierre1-ADCIGs [CR]

result is consistent with the sonic velocity recorded in well 3_9a-8, located at 32.83 km along the CMP axis on line 750. Figure 13 presents the estimates of the interval vertical velocity obtained from surface seismic data, measurement of sonic velocity and checkshot. It illustrates that the vertical velocity estimated from surface seismic data — under the assumption of isotropy — is accurately estimated down to a depth of around 2 km and is overestimated deeper between the Balder and BCU horizons. This overestimation is due to the presence of anisotropic rocks under the Balder layer. The velocity measured from surface seismic data (V_N) is equal to the vertical velocity (V_V) under the assumption of isotropy and flat layers. However, in an anisotropic medium, for flat layers and a VTI model, the expression of the NMO velocity becomes $V_N = V_V\sqrt{1+2\delta}$, where δ is the first Thomsen parameter. Since the velocity measured from seismic data, V_N, is larger than the velocity measured from sonic logs and checkshots, the anisotropic parameter δ probably can not be considered zero and takes significantly positive values.

Finally, we computed anisotropic velocity spectra from the three different ADCIGs illustrated in Figure 12. The first series of velocity spectra are semblance panels of ρ_{V_N} (Figure 14). The velocity spectra are computed by trying to fit the RMO curves in ADCIGs with only ρ_{V_N}. Figure 14 illustrates that the V_N was well estimated by CGG since high semblance values are centered around perturbation values close to zero.

Semblance panels of ρ_{V_H} are presented in a second series of velocity spectra (Figure 15). The second series of velocity spectra is are semblance panels of ρ_{V_H}. The velocity spectra

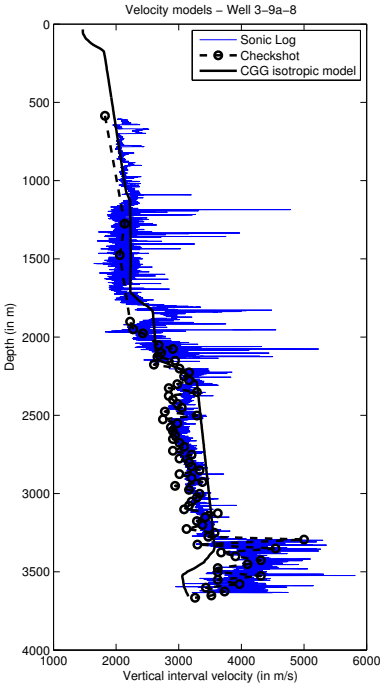

Figure 13: Comparison of the vertical velocities at the location of well 3_9a-8. The different velocities are estimated from seismic surface data (assuming isotropy), measurement of sonic velocity and checkshots. pierre1-Sonic_log [NR]

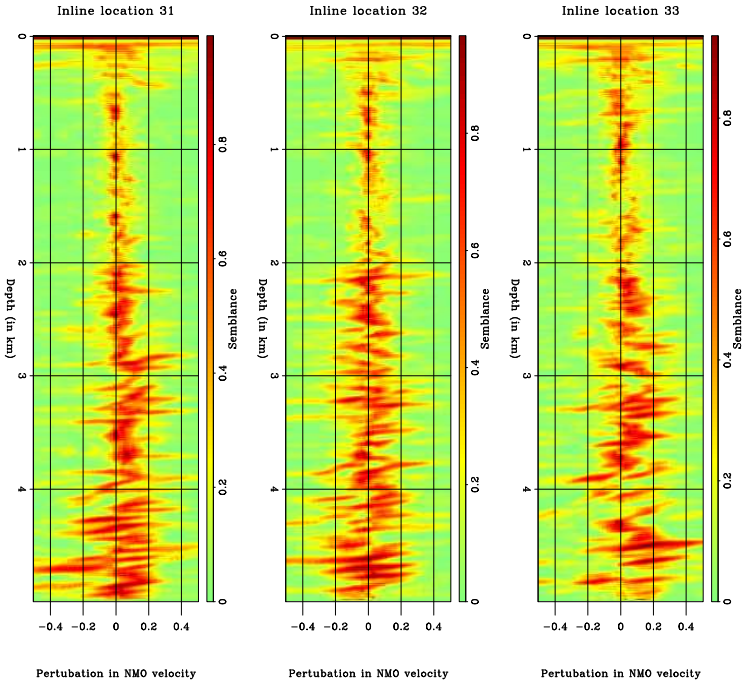

Figure 14: Velocity spectra computed at different inline locations by trying to fit the RMO curves in ADCIGs with only ρ_{V_N}. pierre1-VN_spectra [CR]

are computed by trying to fit the RMO curves in ADCIGs with only ρ_{V_H}, assuming that V_N is correct. Figure 15 illustrates the presence of anisotropy at a depth greater than 2 km. More specifically, the fact that the energy is centered at negative values of the horizontal velocity perturbations indicates that the horizontal velocity we used for the migration is smaller than the true horizontal migration velocity. Since our migration was isotropic, we assumed that $V_H = V_N = V_V$. As a consequence, we can infer that below 2 km depth, the anisotropic parameter ϵ probably should not be set to zero and will take significant positive values ($V_H = V_V\sqrt{1+2\epsilon}$).

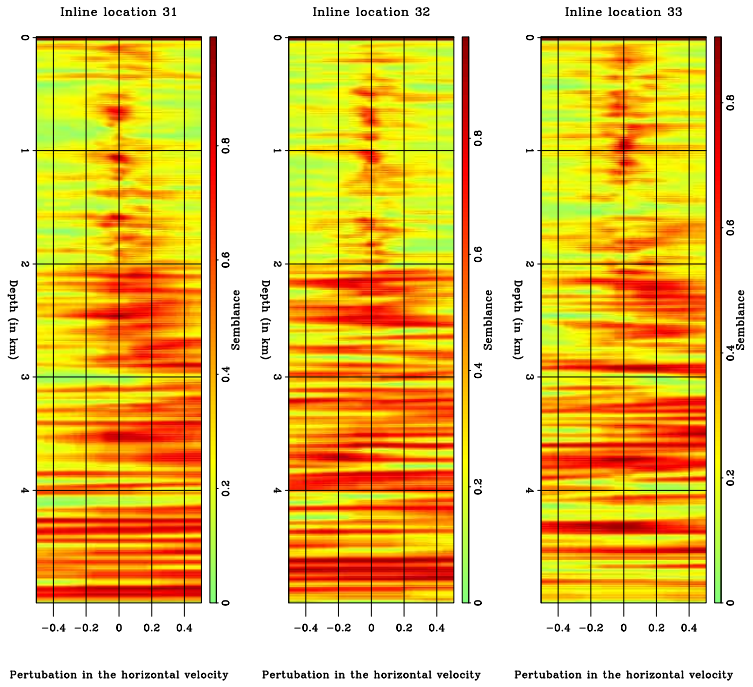

Figure 15: Velocity spectra computed at different inline locations by trying to fit the RMO curves in ADCIGs with only perturbations in the horizontal velocities. pierre1-VH_spectra [CR]

CONCLUSIONS

We presented an anisotropic migration velocity analysis (MVA) method based on the computation and analysis of angle-domain common-image gathers (ADCIGs) in conjunction with anisotropic wavefield-continuation migration. This method is based on the assumption of flat reflectors and vertically transversely isotropic (VTI) media but could also be generalized to dipping reflectors and tilted transversely isotopic (TTI) media. Our method has the great advantage of being based on migrated gathers and allows the iterative estimation of anisotropic parameters. We analyzed synthetic data to determine the accuracy and convergence of the estimation method. We showed that vertical velocities could not be resolved by our method but that even if we used a first-order approximation of the RMO function, picking the anisotropic

migration velocities in semblance panels improves the overall anisotropic parameter estimation. We performed anisotropic MVA on a real data set acquired in the North Sea. Starting from an isotropic velocity model, we demonstrated the validity of our estimation method by showing it indicates the presence of anellipticity in the layers that are stratigraphically interpreted as anisotropic and for which well data do not match seismic data migrated under isotropy assumption.

ACKNOWLEDGMENTS

We would like to thank TOTAL for making the real data set available for SEP through the generous efforts of Jérome Guilbot et Frédéric Joncour.

REFERENCES

Biondi, B. and T. Tisserant, 2004, 3-D angle-domain common-image gathers for migration velocity analysis: Geophisical Prospecting, **52**, 575–591.

Biondi, B., 2005a, Angle-domain common image gathers for anisotropic migration: SEP–**123**.

Biondi, B., 2005b, Residual moveout in anisotropic angle-domain common image gathers: SEP–**123**.

Dellinger, J. and F. Muir, 1985, Two domains of anisotropy: SEP–**44**, 59–62.

Jousselin, P. and B. Biondi, 2006, Residual moveout in anisotropic angle-domain common image gathers with dipping reflectors: SEP–**124**.

Rickett, J. and P. Sava, 2002, Offset and angle-domain common image-point gathers for shot-profile migration: Geophysics, **67**, 883–889.

Sava, P. and S. Fomel, 2003, Angle-domain common-image gathers by wavefield continuation methods: Geophysics, **68**, 1065–1074.

Tsvankin, I., 2001, Seismic Signatures and Analysis of Reflection Data in Anisotropic Media: Elsevier Science.

APPENDIX A

PHASE AND GROUP ANGLES AND VELOCITIES

In anisotropic wave propagation the phase angles and velocities are different from the group angles and velocities. In this appendix we briefly review the concepts of phase and group angles and velocities and the relationships between these physical quantities.

The transformation from phase velocity $\widetilde{V}$ to group velocity V is conventionally defined as the following (Tsvankin, 2001):

$$V = \sqrt{\widetilde{V}^2 + \left(\frac{d\widetilde{V}}{d\widetilde{\theta}}\right)}, \tag{A-1}$$

where $\widetilde{\theta}$ is the phase propagation angle. The associated transformation from phase angles to group angles θ is defined as:

$$\tan\theta = \frac{\tan\widetilde{\theta} + \frac{1}{\widetilde{V}}\frac{d\widetilde{V}}{d\widetilde{\theta}}}{1 - \frac{1}{\widetilde{V}}\frac{d\widetilde{V}}{d\widetilde{\theta}}\tan\widetilde{\theta}}. \tag{A-2}$$

Dellinger and Muir (1985) propose, and heuristically motivate, the following symmetric relations for the inverse transforms:

$$\widetilde{S} = \sqrt{S^2 + \left(\frac{dS}{d\theta}\right)}, \tag{A-3}$$

where $\widetilde{S}$ and S are respectively the phase slowness and the group slowness, and

$$\tan\widetilde{\theta} = \frac{\tan\theta + \frac{1}{S}\frac{dS}{d\theta}}{1 - \frac{1}{S}\frac{dS}{d\theta}\tan\theta}. \tag{A-4}$$

We use the heuristic relation in equation A-4 to derive some of the analytical results presented in this paper. Furthermore, we use all the above relationships to compute the kinematic numerical results presented in this paper.